Sci

MDPI

Article

Spatiotemporal Modelling of Phenology and Population Dynamics of *Halyomorpha halys* in Emilia-Romagna, Italy

Luís Grilo [1,2], José Almeida [1,3], Manuela Simões [1,3,*], Ana Coelho Marques [1,3], Ana Rita F. Coelho [1,3,*] and Lara Maistrello [4]

[1] Earth Sciences Department, NOVA School of Sciences and Technology, Campus de Caparica, 2829-516 Caparica, Portugal; lmmgrilo@gmail.com (L.G.); ja@fct.unl.pt (J.A.); amc.marques@fct.unl.pt (A.C.M.)
[2] Department of Rural Engineering, University of Évora, 7002-554 Évora, Portugal
[3] GeoBioTec Research Center, NOVA University Lisbon, 2829-516 Caparica, Portugal
[4] Department of Life Sciences, University of Modena and Reggio Emilia, 41125 Modena, Italy; lara.maistrello@unimore.it
* Correspondence: mmsr@fct.unl.pt (M.S.); arf.coelho@fct.unl.pt (A.R.F.C.)

Abstract

The brown marmorated stink bug (*Halyomorpha halys*) is a major invasive pest threatening fruit production across Europe. This study integrates spatiotemporal geostatistical modelling with degree-day and photoperiod analyses to characterise its seasonal dynamics in Emilia-Romagna (Italy) from 2020 to 2022. Weekly pheromone trap data were used to quantify developmental succession among Small nymphs (early instars, N1–N3), Large nymphs (late instars, N4–N5), and Adults. Time-series and cross-correlation analyses confirmed consistent developmental delays across years, with Small preceding Large by approximately two weeks and Adults emerging after an additional two to three weeks. However, global inter-stage correlations were moderate ($r \approx 0.4$–0.5), indicating substantial spatial heterogeneity among monitoring sites and suggesting that regional averages do not fully capture local population dynamics. To address this variability, a three-dimensional spatiotemporal geostatistical model (space $\times$ time) was implemented using Direct Sequential Simulation. The model successfully reproduced seasonal population waves and interannual differences in onset and persistence. The identification of persistent hotspots and stage-specific temporal windows is biologically relevant because it highlights where and when *H. halys* populations are most likely to increase. As such, from an IPM perspective, these outputs can support earlier monitoring, more precise timing of management interventions, and spatial prioritization of control efforts. These findings demonstrate that combining stage-specific temporal analysis with spatially explicit modelling improves forecasting accuracy and supports more precise timing of biological and chemical interventions. The proposed framework provides a scalable tool for climate-responsive integrated pest management in fruit-growing systems.

Keywords: brown marmorated stink bug; invasive pest; pheromone trapping; space-time geostatistics; direct sequential simulation; generational dynamics

Academic Editor: Franca Rossi

Received: 30 April 2026
Revised: 26 June 2026
Accepted: 27 June 2026
Published: 7 July 2026

1. Introduction

Halyomorpha halys Stål, 1855, also known as the brown marmorated stink bug (BMSB), is a polyphagous agricultural pest native to east Asia, particularly China, Japan, Korea, and Taiwan [1,2]. Over the past three decades, it has become a globally invasive species,

significantly impacting agricultural production across North America and Europe [3–5]. In Europe, it was first detected in Switzerland in 2004 and subsequently established in Italy (2007), France (2012), and Spain (2016) [6]. By 2019, the species had been reported in more than 15 European countries [7,8], and recent surveys confirm its continued spread, including updated data on distribution and genetic diversity in Europe [9,10]. Genetic analyses indicate multiple introduction events and substantial gene flow, reflecting strong dispersal capacity and adaptive potential.

BMSB feeds on and reproduces across more than 300 ornamental and agricultural plant species [10–12]. While in its native range, it is often an occasional outbreak species with limited economic relevance [13], its invasion of new continents has resulted in major agricultural losses. Feeding through piercing–sucking mouthparts damages fruits and seeds, reducing quality and marketability [3]. Economically important hosts include apple (*Malus domestica*), pear (*Pyrus communis*), peach (*Prunus persica*), grape (*Vitis vinifera*), soybean (*Glycine max*), and tomato (*Solanum lycopersicum*) [12,14]. Contamination of grape harvests may also cause off-flavours in wine at low concentrations [15].

The economic impact of BMSB has been substantial. In the United States, severe outbreaks caused major orchard losses within 15 years of introduction [16]. In Europe, Italy has been among the most-affected countries, with the Emilia-Romagna region experiencing severe damage, including losses approaching EUR 600 million in 2019 [10]. Updated assessments place BMSB among the invasive species associated with the highest hidden economic costs in the European Union [17]. These impacts underscore the need for improved monitoring and sustainable management strategies.

Emilia-Romagna represents an ideal setting for investigating the spatiotemporal dynamics of BMSB because it combines intensive fruit production, a history of severe infestations and economic damage, and an established long-standing regional monitoring network. This network has been active since the very first detection of the invasive pest in the Italian territory [10]. Therefore, the region can be considered both an invasion-impact hotspot and a monitoring-intensive agricultural landscape.

The BMSB overwinters as an Adult in reproductive diapause, with spring emergence and reproductive activation mainly regulated by temperature and photoperiod. After mating (Figure 1A), females lay egg masses (Figure 1B) and development proceeds through five nymphal instars (Figure 1C–G) before adulthood (Figure 1H). Developmental rates are temperature-dependent, and in northern Italy the species commonly completes two generations per year [10]. Also, because diapause termination, reproduction, and stage progression are strongly linked to seasonal conditions, stage-specific monitoring is essential for understanding population dynamics and improving the timing of IPM interventions [13,14].

At the end of the growing season, decreasing photoperiod and temperature trigger the onset of diapause. Adults cease reproduction and feeding, and migrate to overwintering sites, where they remain aggregated and largely inactive until the following spring. Overall, post-diapause emergence and seasonal population dynamics are closely linked to temperature and photoperiod, making BMSB phenology highly responsive to climatic variability [18,19].

Although several studies have described the biology, phenology, and distribution of BMSB, fewer have quantified how stage-specific population dynamics vary simultaneously across space and time at a regional scale. In particular, regional averages can describe general seasonal trends but may fail to detect local asynchrony, persistent hotspots, and spatial differences in developmental timing. This represents an important gap for IPM, because control actions are often implemented locally and depend on the correct timing of vulnerable life stages.

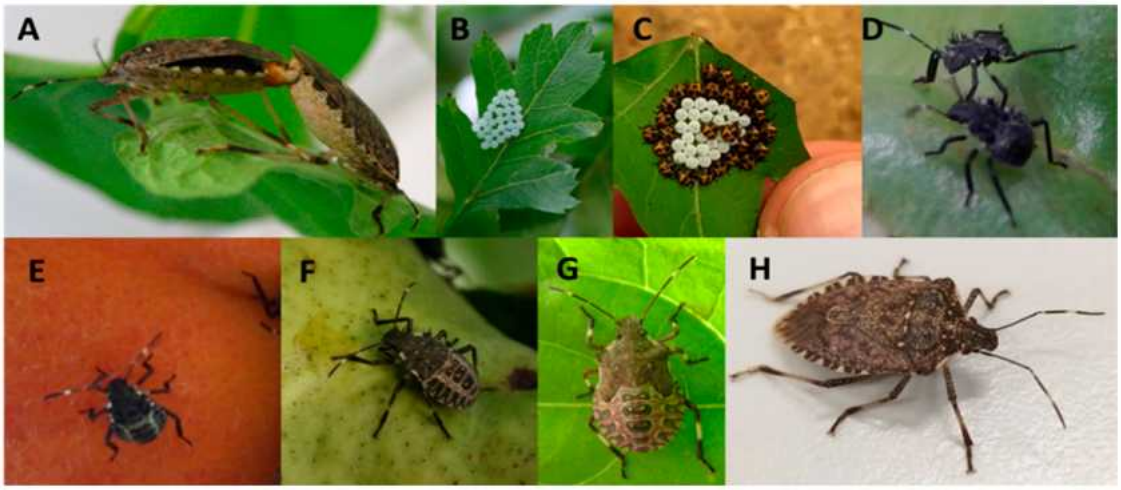

Figure 1. Different stages in the BMSB life cycle. (**A**) mating; (**B**) egg mass; (**C**) egg hatching/first instar; (**D**) second instar; (**E**) third instar; (**F**) fourth instar; (**G**) fifth instar; (**H**) adult. Source: Pictures from Laboratory of Entomology, University of Modena and Reggio Emilia (UNIMORE).

Understanding the ecological and climatic drivers of population dynamics is essential for developing predictive management frameworks. Because BMSB responds strongly to temperature, accurate characterization of stage-specific phenology is critical for optimizing the timing of biological control releases and insecticide applications. Despite extensive monitoring networks across Europe, high-resolution multi-year analyses integrating stage-specific phenology and spatial variability remain limited at the regional scale. Moreover, interannual climatic variability may alter seasonal development patterns and pest pressure.

Monitoring plays a central role in integrated pest management (IPM) strategies. Pheromone-baited traps are the primary surveillance tool and are increasingly integrated with digital monitoring frameworks and spatial modelling approaches [20,21]. These systems generate the spatial datasets required for predictive modelling [22].

Control remains challenging due to high mobility, broad host range, and reproductive potential. Chemical control is limited by environmental concerns [23]. Biological control, particularly through the establishment of *Trissolcus japonicus* and other scelionid parasitoids, represents a promising sustainable strategy, although its effectiveness depends on climatic synchrony and landscape context [10,24,25].

Recent advances in spatiotemporal and degree-day modelling have improved understanding of BMSB dynamics in invaded regions [26]. In Emilia-Romagna, coordinated monitoring between 2020 and 2022 generated high-resolution datasets suitable for geostatistical and phenological analyses [22]. These tools support prediction of phenological milestones and regional spread, improving the timing of control actions.

This study builds on these efforts by integrating field monitoring data with spatiotemporal geostatistical modelling to analyse the seasonal population dynamics of BMSB in northern Italy, with the ultimate aim of refining predictive capacity for sustainable pest management strategies. Specifically, we hypothesized that different life stages would exhibit distinct spatiotemporal patterns driven by their ecological and behavioural traits. Adults were expected to display broader spatial and temporal continuity due to their flight capability, high mobility, and longer seasonal persistence. In contrast, Small instars were hypothesized to show more localized, fragmented distributions, reflecting their limited mobility, strong reliance on maternal oviposition sites, and higher vulnerability to early-stage environmental mortality.

2. Materials and Methods

2.1. Study Area

The study was conducted in Emilia-Romagna, northern Italy, a major fruit-producing region extending from the Po River plain to the foothills of the northern Apennines (Figure 2). The study area covers approximately 663,912 ha across the main fruit-growing districts of Modena, Ferrara, Bologna, and Ravenna. The central coordinate of the area of study is 44.7087, 11.3784.

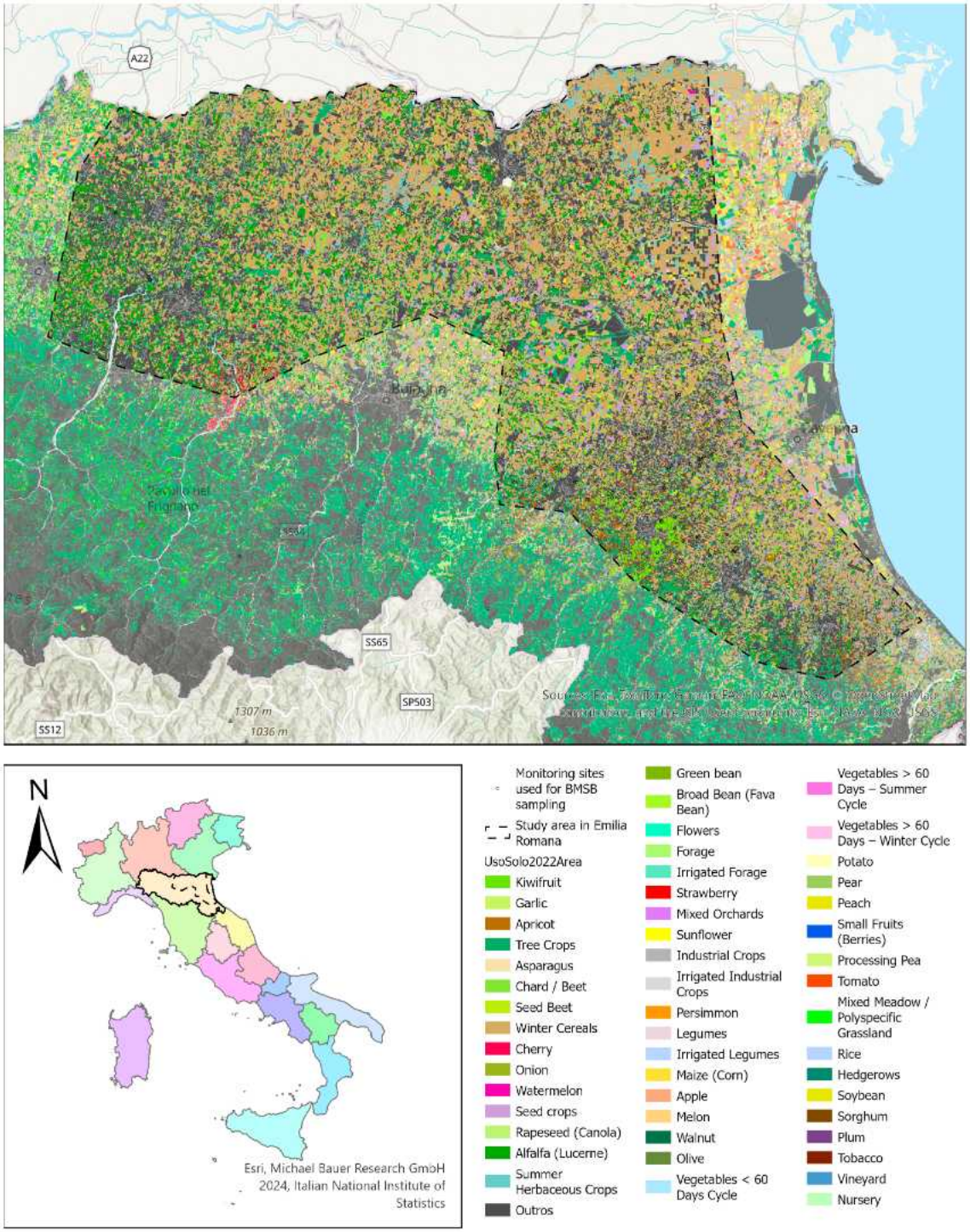

Figure 2. Location of the study area in Emilia-Romagna, northern Italy, and land use in the study area (more than 600,000 hectares), highlighting the main fruit and arable crop systems associated with BMSB host availability.

Emilia-Romagna produces more than 1.3 million tonnes of fruit annually. The main crops include pear (*Pyrus communis*), grape (*Vitis vinifera*), apple (*Malus domestica*), peach (*Prunus persica*), and cherry (*Prunus avium*). Field crops such as soybean (*Glycine max*), maize (*Zea mays*), and wheat (*Triticum aestivum*) are also widely cultivated across the plains. Orchard margins and hedgerows frequently contain wild host plants, including *Ailanthus altissima* and *Robinia pseudoacacia*, which may serve as refuges and overwintering sites for the pest [3].

The area was selected due to its well-established monitoring networks, high orchard density, and the severe infestations of BMSB recorded since 2015, making it a suitable region for analysing the spatiotemporal dynamics of this species under field conditions [3,10]. Monitoring sites are predominantly located within the flat agricultural landscape, reflecting the spatial distribution of intensive fruit production systems.

Emilia-Romagna, with an average altitude of 24.28 m above sea level (Figure 3)—reaching up to approximately 200 m in the southern areas—has a humid subtropical climate (Cfa), with an average annual temperature of 15.9 °C (60.6 °F), annual mean highs of 19.1 °C and lows of 10.0 °C. Summers are hot, peaking at 31.4 °C in August, while winters are cold, dropping to 1.7 °C in January. Annual precipitation averages 43.14 mm (wettest in May and driest in January), with approximately 87 rainy days per year and a mean relative humidity of 71% (ARPAE [27]) (Figure 4). These climatic conditions favour fruit cultivation and are also suitable for the development and overwintering of BMSB.

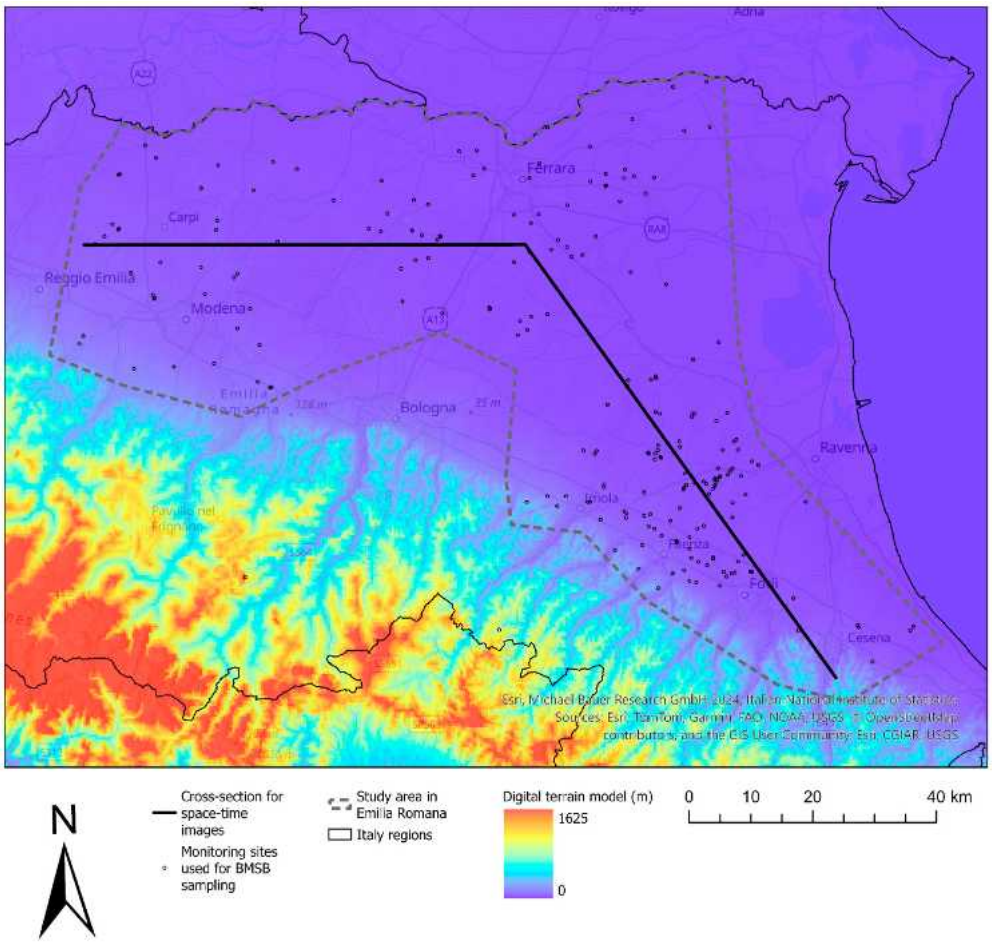

Figure 3. Digital terrain model of the studied area. Data source: World Elevation GMTED.

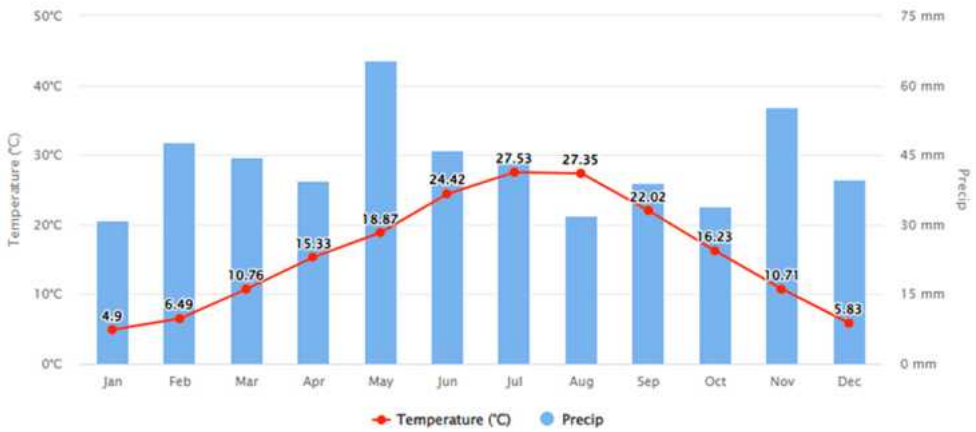

Figure 4. Mean monthly air temperature (°C) (red line) and cumulative monthly precipitation (mm) for the period 2000–2020 in Emilia-Romagna (Italy). Data provided by ARPAE [27]. Red line with markers: Temperature (°C); blue bars: Precipitation (mm).

2.2. Monitoring Network and Field Data Collection

Monitoring data of BMSB were collected from 2020 to 2022 through a regional network (https://big.csr.unibo.it/projects/cimice/, accessed on 29 April 2026; [22]) of pheromone-baited traps distributed across the main fruit-growing districts of Emilia-Romagna. Traps were installed in pear, apple, and peach orchards, as well as along hedgerows bordering cultivated fields, at approximately 1.5–2.0 m above ground. Each trap consisted of a double-cone design (Trécé Inc., Adair, OK, USA) baited with an aggregation pheromone lure replaced every 90 days, as indicated by the manufacturer. Captures were recorded as the number of individuals per trap per week, providing a direct measure of local abundance.

A largely consistent set of orchards was monitored each year, although specific trap locations varied slightly due to crop rotation and management constraints. Trap coordinates were georeferenced in the WGS84 coordinate system and verified in ArcGIS Pro (version 3.6). Overall, 235 trap locations were included in the dataset, with 132 traps active in 2020, 156 in 2021, and 77 in 2022, totalling 365 trap-years of observations (Figure 5).

Captured specimens were classified as Small (early instars, N1–N3), Large (late instars, N4–N5), and Adults based on body size and wing development, following Maistrello et al. (2017) [3]. This distinction allowed the assessment of population structure and seasonal dynamics, particularly the timing of new generation emergence. The resulting dataset provided weekly counts of BMSB Adults and nymphs per trap, forming the empirical basis for the phenological and spatiotemporal analyses described in the following sections.

2.3. Statistical and Time-Series Analysis

Prior to the construction of the space–time geostatistical model, exploratory time-series analyses were conducted to characterise the seasonal dynamics of BMSB populations and to identify temporal and spatial patterns across the monitoring network. Weekly counts of Small, Large, and Adults per trap were used as the basic time-series units for the three-year dataset. Outliers were visually inspected and removed when associated with trap malfunction or incomplete sampling.

A table of descriptive statistics was compiled for each year and life stage (Small, Large, and Adults), including mean, median, minimum, maximum, coefficient of variation, and skewness. These metrics allowed a comparative assessment of interannual variability, dispersion, and asymmetry in population distributions.

Seasonal trends were further examined by plotting weekly time series of abundances for each life stage and year. The temporal patterns were interpreted in terms of onset of population increase, timing and magnitude of peaks, decline phases, and the area under

successive increases and decreases in abundance. These features were compared among years to evaluate differences in phenology and population intensity.

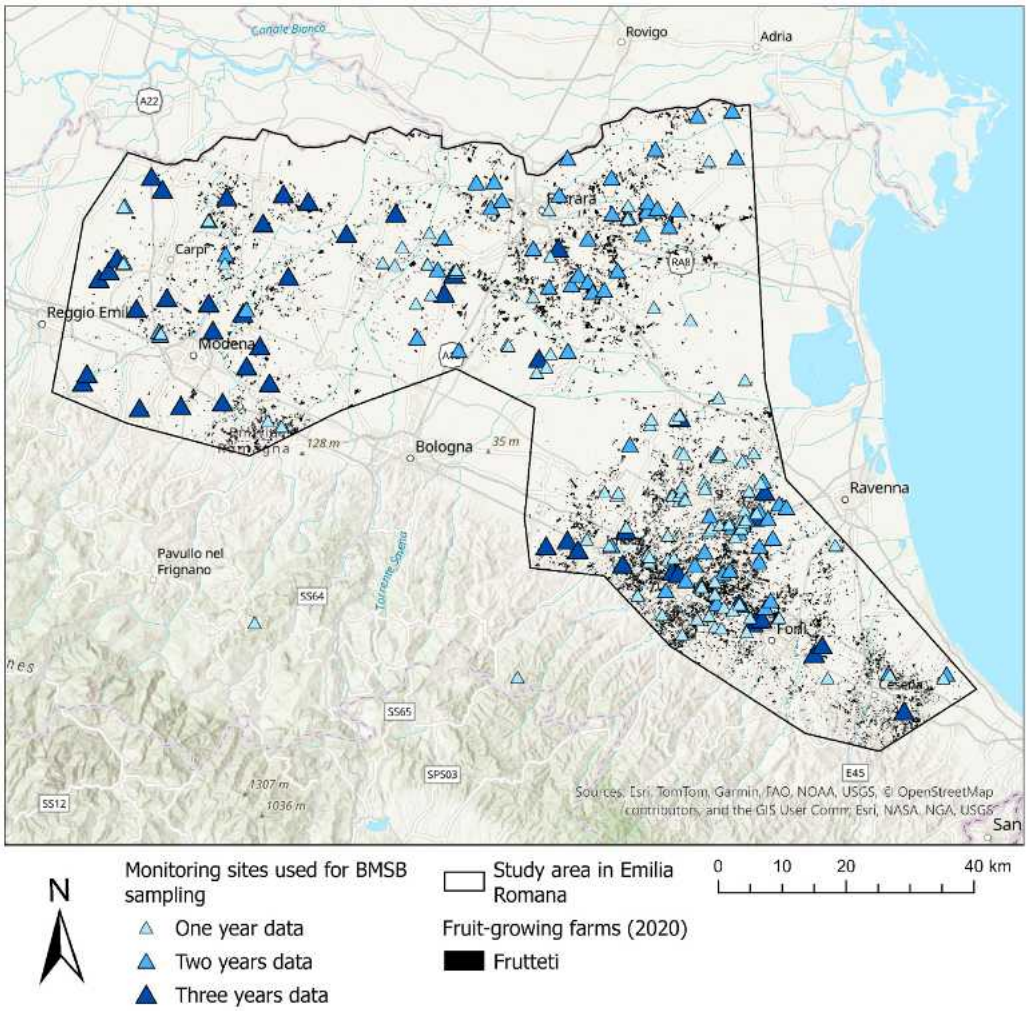

Figure 5. Location of the study area and pheromone trap network in Emilia-Romagna (2020–2022)—central coordinates: 44.7087, 11.3784.

For each year, peak week was identified and temporal delays between stages were estimated, allowing visual and quantitative assessment of developmental lags. Correlation coefficients were computed to confirm relationships between consecutive developmental stages (Small vs. Large and Large vs. Adults). Differences in peak magnitude and timing among locations were examined to evaluate spatial heterogeneity in population build-up and generational turnover.

2.4. Spatiotemporal Geostatistical Model

Geostatistical approaches, including interpolation techniques such as kriging and stochastic simulation methods, have become key tools in ecological studies for mapping species distributions and capturing spatial variability, particularly in the context of insect population dynamics and pest management [28–30].

A spatiotemporal geostatistical model was developed in which time was explicitly incorporated as a third dimension in addition to the two spatial coordinates. In this framework, the variable of interest $Z(s,t)$ is defined over a three-dimensional domain, where $s = (x,y)$ represents spatial location and t represents time (week). This approach enables the joint modelling of spatial aggregation and temporal continuity, allowing the identification of structured dependence across both space and time [31].

Directional structure considered two spatial axes and one temporal axis. Spatiotemporal dependence was quantified using experimental semi-variograms computed in three dimensions as [32,33]:

$$\gamma(h_s, h_t) = \frac{1}{2N(h_s, h_t)} \sum_{i=1}^{N(h_s,h_t)} [Z(s_i, t_i) - Z(s_i + h_s, t_i + h_t)]^2 \quad (1)$$

where h_s and h_t represent spatial and temporal lags, respectively. Separate variograms were computed for each developmental stage (Small, Large, and Adults), combining the three monitoring years into a single model to characterise the overall spatiotemporal structure of population dynamics. Experimental variograms were fitted with appropriate theoretical models to estimate nugget, sill, and spatial and temporal ranges.

Instead of deterministic interpolation methods such as ordinary kriging, direct sequential simulation (DSS) was used to generate the spatiotemporal model [34,35]. DSS is particularly suitable in this context because repeated observations occur at identical spatial coordinates across multiple weeks, a situation that may introduce artefacts or excessive smoothing under kriging. Moreover, DSS allows straightforward conditioning to external constraints, such as the observed weekly global means, thereby reinforcing temporal consistency in the simulations. By conditioning each step to both the fitted spatiotemporal variogram and the empirical weekly averages, the procedure preserves local variability while maintaining coherence with the overall seasonal signal.

Multiple equiprobable realisations were generated independently for each developmental stage. The ensemble of simulations was then used to derive mean predicted abundance and associated uncertainty (standard deviation) at each grid node, enabling the explicit mapping of both expected pest intensity and prediction uncertainty across the study domain.

3. Results

3.1. Exploratory Data Analysis

Descriptive statistics revealed interannual variability and strongly right-skewed distributions across all developmental/life stages of BMSB (Table 1 and Figure 6). The weekly mean of Adults ranged from 8.47 (in 2021) to 10.76 (in 2020), while Small individuals showed a clear decline from 5.74 (in 2020) and 4.28 (in 2021) to only 2.77 (in 2022), corresponding to an about 52% reduction between 2020 and 2022. Also, in the category of Large, it is possible to observe that they consistently showed lower mean values across all years (1.25 to 2.13) which could reflect their shorter development window. Coefficients of variation were high (Table 1), particularly for nymphal stages, indicating pronounced temporal and spatial heterogeneity. Skewness values consistently exceeded 2, reflecting the occurrence of episodic population peaks.

After excluding zero counts, mean values increased (namely, Adults from 10.76 to 15.36 in 2020), while coefficients of variation decreased across all stages, indicating that a substantial proportion of variability was associated with weeks or locations without captures.

The weekly time series exhibited a clear and recurrent seasonal pattern across the three years (Figure 6), characterised by distinct population increases followed by rapid declines. Adults were consistently the first stage detected each season, preceding the rise of nymphal stages, consistent with the post-diapause emergence of overwintered individuals after reaching the species-specific degree-day threshold required for reproductive activation.

Table 1. Basic descriptive statistics of weekly BMSBcounts by year and developmental stage, calculated with and without zero values: mean (m), median (M), minimum (min), maximum (max), coefficient of variation (CV) and skewness (SK).

Description	Year	Stage	#	m	M	Min	Max	CV	SK
All data	2020	Adults	3099	10.76	3.0	0	145	1.638	2.459
		Large	3099	2.13	0.0	0	66	2.393	4.358
		Small	3099	5.74	0.0	0	305	3.274	7.502
	2021	Adults	4696	8.47	2.0	0	266	1.843	5.128
		Large	4696	1.47	0.0	0	68	3.176	6.018
		Small	4696	4.28	0.0	0	240	3.084	6.564
	2022	Adults	2660	9.18	2.0	0	186	1.929	3.555
		Large	2660	1.25	0.0	0	79	3.565	7.553
		Small	2660	2.77	0.0	0	119	2.978	6.070
Remove zeros	2020	Adults	2171	15.36	7.0	1	145	1.257	2.016
		Large	1019	6.48	4.0	1	66	1.101	2.840
		Small	1073	16.57	7.0	1	305	1.749	4.745
	2021	Adults	3045	13.07	7.0	1	266	1.361	4.627
		Large	1094	6.31	4.0	1	68	1.258	3.220
		Small	1389	14.45	7.0	1	240	1.452	3.952
	2022	Adults	1670	14.62	6.0	1	186	1.401	2.893
		Large	585	5.70	3.0	1	79	1.420	3.986
		Small	785	9.37	5.0	1	119	1.383	3.643

Figure 6. Weekly mean captures of BMSB Adults and nymphal stages (Small: N1–N3; Large: N4–N5) in 2020, 2021, and 2022. Curves show seasonal dynamics and developmental succession among life stages.

In all years, two major population increases were observed within the growing season. This apparent bimodal pattern may reflect the occurrence of successive generations under field conditions; however, it may also partly result from spatial asynchrony among

monitoring locations, where slight differences in phenology across sites generate aggregated multi-peak patterns when averaged at the regional scale. Small showed sharp and temporally concentrated peaks, followed by Large with a consistent developmental lag of approximately 1–2 weeks, and subsequently by Adults with an additional delay of 1–3 weeks. Adult captures frequently displayed broader or secondary peaks, suggesting partial generational overlap and sustained oviposition (Table 2).

Table 2. Phenological metrics of *BMSB* life stages (Small: N1–N3; Large: N4–N5; Adults) across 2020–2022, including onset, peak, end, duration, centre of gravity in time (CGT), and seasonal area under the curve, calculated for the full activity period and for the central 10–90% activity window.

		All Weeks						Remove Extremes (10–90%)			
	Year	**Onset**	**Peak**	**End**	**Duration**	**CGT**	**Area**	**Onset**	**Peak**	**End**	**Duration**
Small	2020	23	35	41	19	33.66	140.4	28	35	37	10
	2021	21	33	41	21	30.77	133.4	25	33	35	11
	2022	22	34	41	20	31.46	78.9	25	34	36	12
Large	2020	26	37	42	17	35.6	51.2	30	37	39	10
	2021	25	36	42	18	33.8	47.4	28	36	38	11
	2022	24	37	42	19	34.69	36.9	29	37	38	10
Adults	2020	18	41	42	25	37.15	263.8	31	41	42	12
	2021	11	39	42	32	34.05	281.8	22	39	41	20
	2022	13	40	42	30	34.9	281.5	21	40	41	21

Phenological metrics (Table 2) showed strong interannual consistency and clear stage succession. Adults exhibited the earliest onset (weeks 11–18), followed by Small (weeks 21–23) and Large (weeks 24–26). Peak timing was highly stable, occurring around weeks 33–35 for Small, 36–37 for Large, and 39–41 for Adults. The interval between peaks indicated an average delay of ~2 weeks from Small to Large and an additional 2–3 weeks to Adults, consistent with temperature-driven developmental progression.

Seasonal duration was longest for Adults (25–32 weeks) and shorter for nymphs (17–21 weeks). When considering the central 10–90% activity window, duration decreased markedly for nymphal stages (10–12 weeks), whereas Adults retained a broader window (12–21 weeks), suggesting prolonged activity and possible generational overlap. Seasonal area was highest for Adults and lowest for Large, with a noticeable reduction in Small abundance in 2022 compared with previous years.

3.2. Bivariate Correlations

Bivariate relationships between consecutive developmental stages were analysed using Pearson and Spearman correlation coefficients constructed for Small vs. Large, Large vs. Adults, and Small vs. Adults (Table 3). The analysis was performed separately for each monitoring station, and week delays were calculated for each year to preserve local phenological structure.

Table 3. Inter-stage peak delays (weeks) between developmental stages of BMSB, calculated from seasonal peak timing.

Year	**Large–Small**	**Adults–Large**	**Adults–Small**
2020	2	4	6
2021	3	3	6
2022	3	3	6

For each stage pair, values were matched using a temporal lag corresponding to the average difference in peak timing between the two stages. Weekly counts of the earlier stage (e.g., Small) were paired with counts of the subsequent stage (e.g., Large) shifted forward by the mean number of weeks separating their seasonal peaks. This lag-adjusted pairing accounts for the typical developmental delay between stages and enables a biologically meaningful comparison of generational progression. Table 3 provides a list of the inter-stage peak delays (weeks) between developmental stages of BMSB and Table 4 presents the Pearson and Spearman cross-correlation coefficients. Positive lags indicate that the first variable precedes the second variable by the specified number of weeks. The number of stations included in each calculation is shown for each year and lag.

Table 4. Mean Pearson (PC) and Spearman (SC) cross-correlations between life-stage counts (Small, Large, and Adults) calculated across monitoring stations for weekly lags ranging from 0 to 7 weeks within each year (2020–2022).

Stage	Week Lag	2020			2021			2022		
		PC	SC	#	PC	SC	#	PC	SC	#
Large → Adults	0	0.34	0.48	137	0.26	0.38	149	0.32	0.39	90
	1	0.38	0.49	137	0.34	0.40	147	0.37	0.40	89
	2	0.47	0.51	136	0.41	0.46	145	0.46	0.44	88
	3	0.47	0.51	133	0.41	0.46	145	0.45	0.42	87
	4	0.42	0.47	132	0.35	0.43	144	0.37	0.37	83
	5	0.37	0.42	131	0.31	0.40	144	0.30	0.33	75
	6	0.32	0.37	123	0.28	0.37	136	0.26	0.30	72
	7	0.31	0.37	116	0.26	0.33	130	0.22	0.27	64
Small → Large	0	0.34	0.44	133	0.31	0.45	148	0.22	0.33	90
	1	0.38	0.46	133	0.31	0.47	147	0.27	0.40	90
	2	0.39	0.47	133	0.40	0.53	146	0.40	0.48	90
	3	0.31	0.39	133	0.39	0.50	145	0.28	0.39	90
	4	0.19	0.29	133	0.32	0.43	145	0.26	0.34	90
	5	0.09	0.21	133	0.22	0.37	145	0.18	0.27	90
	6	0.03	0.15	133	0.12	0.28	144	0.14	0.21	89
	7	−0.01	0.10	131	0.08	0.23	143	0.07	0.16	86
Small → Adult	0	0.05	0.22	133	0.03	0.17	154	0.02	0.11	98
	1	0.09	0.26	133	0.06	0.18	153	0.05	0.13	97
	2	0.18	0.32	133	0.13	0.26	152	0.12	0.20	96
	3	0.30	0.41	133	0.21	0.32	151	0.21	0.25	96
	4	0.39	0.47	133	0.31	0.39	151	0.28	0.31	96
	5	0.45	0.50	133	0.37	0.44	151	0.34	0.36	94
	6	0.42	0.47	133	0.34	0.43	150	0.35	0.37	93
	7	0.35	0.44	132	0.31	0.41	149	0.30	0.32	90

The Pearson and Spearman cross-correlations (Table 4) calculated for weekly lags (0–7 weeks) confirm the temporal delays previously identified in the time-series analyses. Across the three study years (2020–2022), increases in Small individuals consistently preceded increases in Large individuals by approximately two weeks, while Large individuals

preceded Adults by an additional two to three weeks. The cumulative delay from Small to Adults was therefore approximately four to six weeks. However, the highest correlations observed between stages in any given year were generally moderate ($r \approx 0.4–0.5$). Although consistent in timing, these values indicate substantial heterogeneity among monitoring stations. The strength of association between stages varied spatially, and stage-specific counts did not always reflect clear growth–decline transitions at the local scale.

This spatial heterogeneity suggests that mean cross-correlation patterns provide a useful global description of stage succession but remain incomplete for local interpretation. Consequently, a three-dimensional geostatistical modelling framework (space $\times$ time) for stage-specific counts is justified. Such an approach would allow spatially explicit characterization of developmental dynamics, capturing local variability that is not represented in average temporal correlations.

The moderate inter-stage correlations indicate that the developmental sequence was consistent at the regional scale but not uniform across monitoring sites. This spatial heterogeneity is biologically meaningful because local host availability, oviposition sites, microhabitat conditions, and Adult dispersal may generate asynchronous population development. As such, consequently, regional averages alone may mask local hotspots and phenological differences that are important for targeted management.

3.3. Spatiotemporal Model

A stochastic geostatistical spatiotemporal model of counts was developed for the Small and Adult life stages for the three study years (2020, 2021, and 2022).

3.3.1. Variograms

Spatial and temporal variograms were computed for life stages Small and Adults and are displayed in Figure 7. The models of variograms (two imbricated structures for the space model) indicate that Adults exhibit greater spatial and temporal continuity, with dominant long-range structures (up to 100 km and 20 weeks), whereas Smalls display more localized and short-term variability (up to 12,5 km and 6 weeks), reflecting weaker continuity in both space and time. The first structure with very low range, 2500 m and 500 m, acts as a spatial nugget effect, and is caused by abrupt transitions between zeros and non-zeros counts.

3.3.2. Spatiotemporal Model of Smalls and Adults

Direct Sequential Simulation (DSS) constrained by local weekly count measurements, weekly count histograms, and variograms was applied to generate a set of 500 equiprobable realizations of Adults and Small counts, from which mean and variance maps were computed for prediction and uncertainty assessment. Validation was performed to confirm the consistency between the true and simulated data. The results showed that the variograms of the simulated images closely matched the modelled variograms, and the basic statistical properties, including the mean and variance, were in good agreement. As such, Figure 8 presents 3D views of the mean maps for both models (Small and Adults). Moreover, Figure 8 shows a clear difference between the development stages, with Adult populations displaying a greater spatial continuity, forming broader and more connected high-density areas across the study region in Emilia-Romagna (Figure 8A). However, in contrast, Small individuals (Figure 8B) exhibit a more "fragmented" and a higher spatial variability. Moreover, the temporal dimension further indicates a stage-specific dynamics, with Adult populations persisting across a wider range of time steps, which can indicate a more prolonged seasonal activity, whereas the Smalls are confined to a shorter temporal window, which can reflect their limited development duration. Additionally, it is possible to observe that high abundance zones are more widespread and consistent for Adults, while

Small appears to be more intermittent and spatially restricted, and despite interannual variability occurs, some regions consistently show higher population levels, which suggests the presence of persistent hotspots within the landscape. As such, the patterns observed demonstrate that the spatiotemporal model effectively captures both large-scale continuity and even local variability.

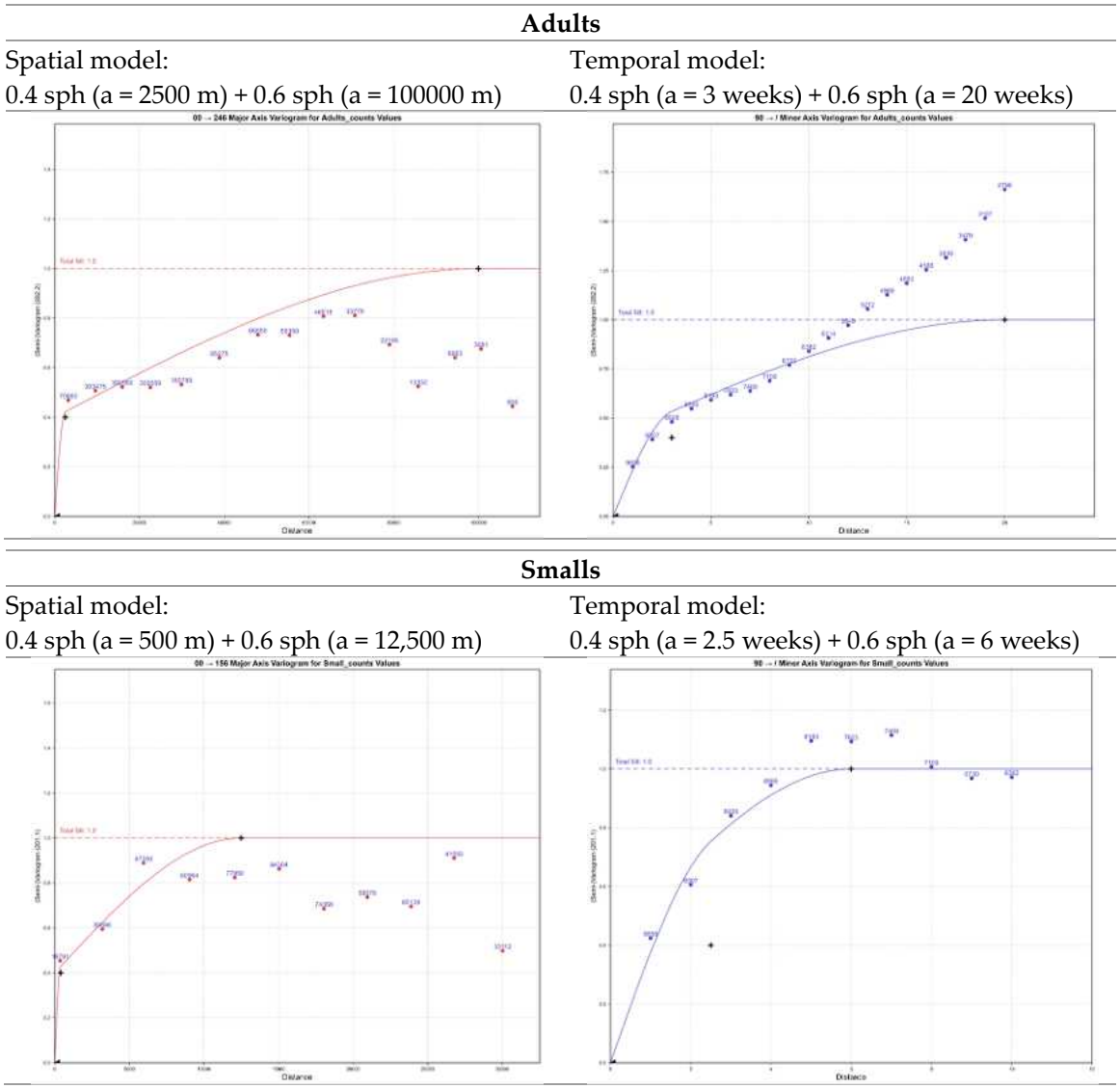

Figure 7. Experimental variograms and fitted spherical models (sph) for the Small and Adult life stages, in both spatial and temporal (weekly) domains (solid line indicates the empirical variogram trend; + marks indicate the lag-bin centers; dots/points indicates the values contributing to each lag class).

In Figure 9, an intermediate east–west cross-section is presented, displaying one realization together with the corresponding mean and variance maps for both Small (left) and Adult (right) stages. Moreover, a clear temporal structure can be observed in both stages, with distinct horizontal bands corresponding to seasonal populations peaks, and these bands are consistent across years which indicates stable and recurrent phenological dynamics. In fact, differences between development stages are verified, with Adult populations exhibiting broader and more continuous temporal bands (i.e., reflecting longer persistence throughout the season), while Small-stage populations show more irregular bands (i.e., indicating a shorter and more sporadic occurrence). As such, the cross-section

confirms that the spatiotemporal model captures both the temporal organization and the stage-specific differences and variability of BMSB populations.

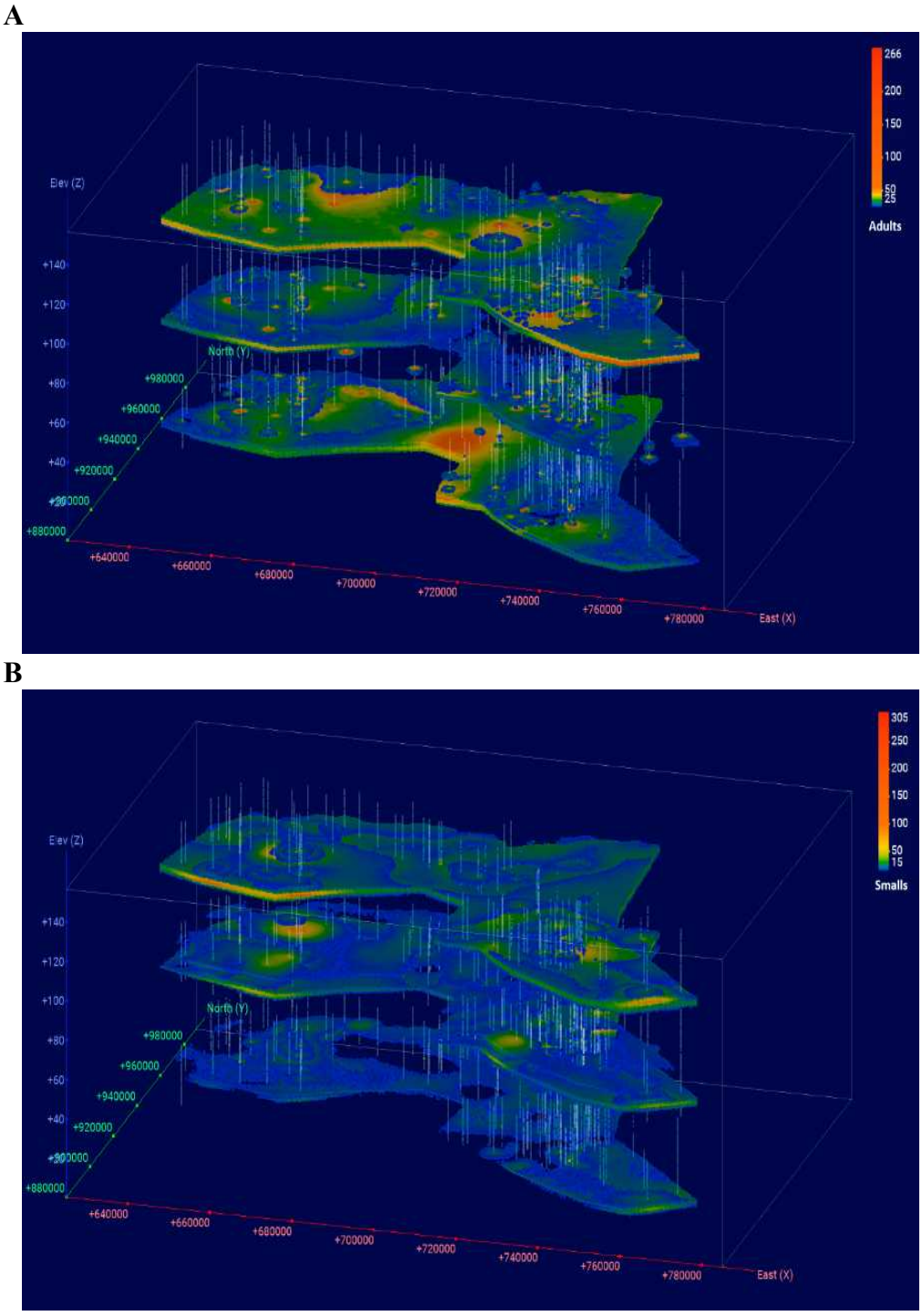

Figure 8. 3D views of average simulated counts for Adult (**A**) and Small (**B**) stages in the Emilia-Romagna region across the three study years, using minimum thresholds of 15 (Small) and 25 (Adult).

Figures 10 and 11 provide aerial views highlighting, for each year (2020, 2021, and 2022), respectively, the maximum number of Adults counts observed in each year, as well as the week when Adults counts begin to appear.

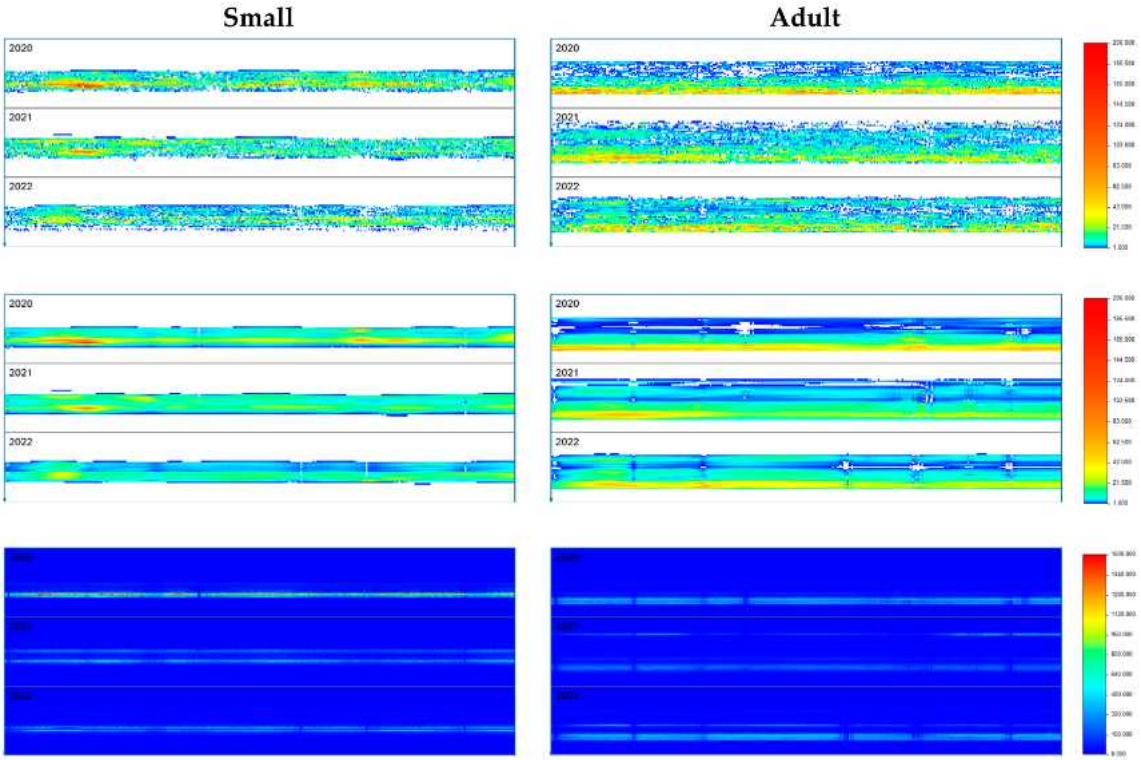

Figure 9. Intermediate east–west cross-section over the three study years (vertical axis corresponds to time), showing one realization together with the corresponding mean and variance maps for the Small (**left**) and Adult (**right**) stages.

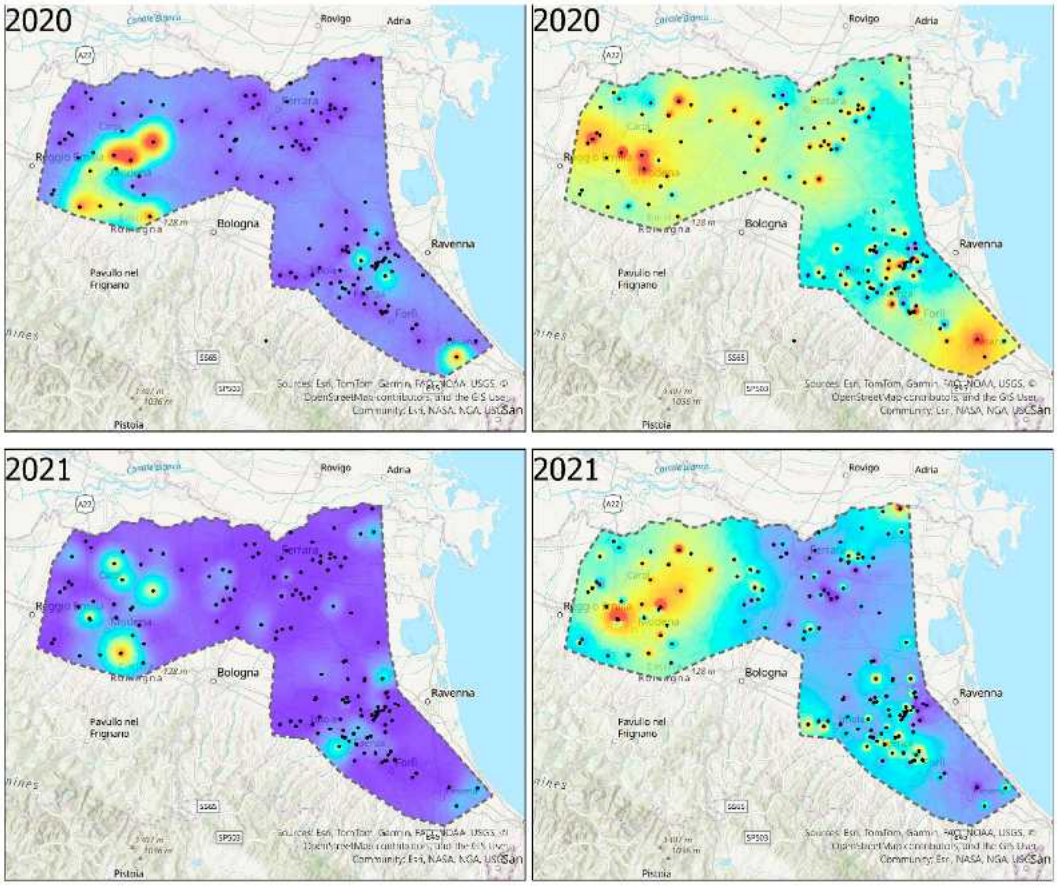

Figure 10. *Cont.*

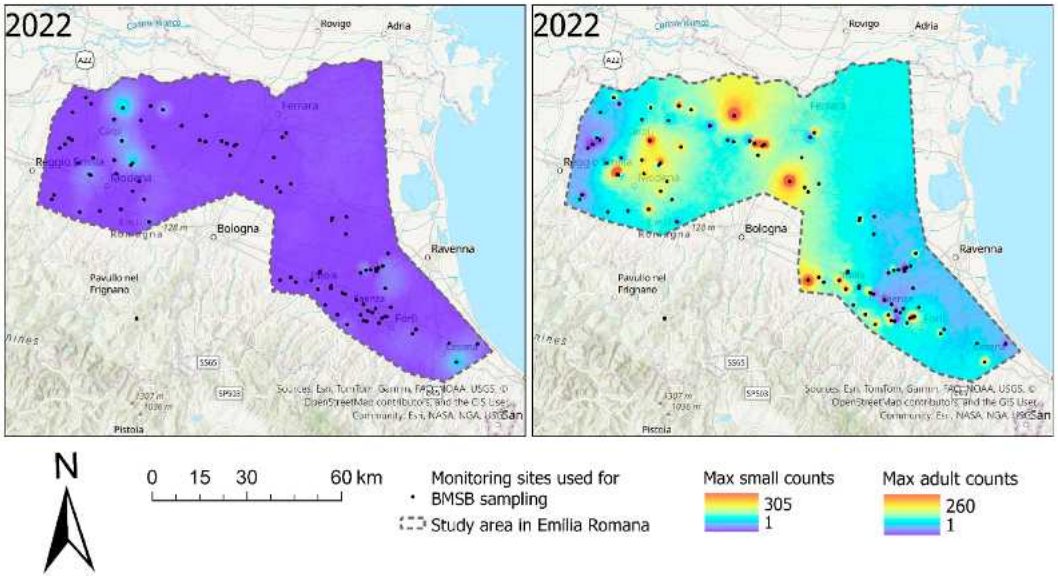

Figure 10. Spatial distribution of maximum counts per year for Small (**left panels**) and Adult (**right panels**) individuals in 2020, 2021, and 2022.

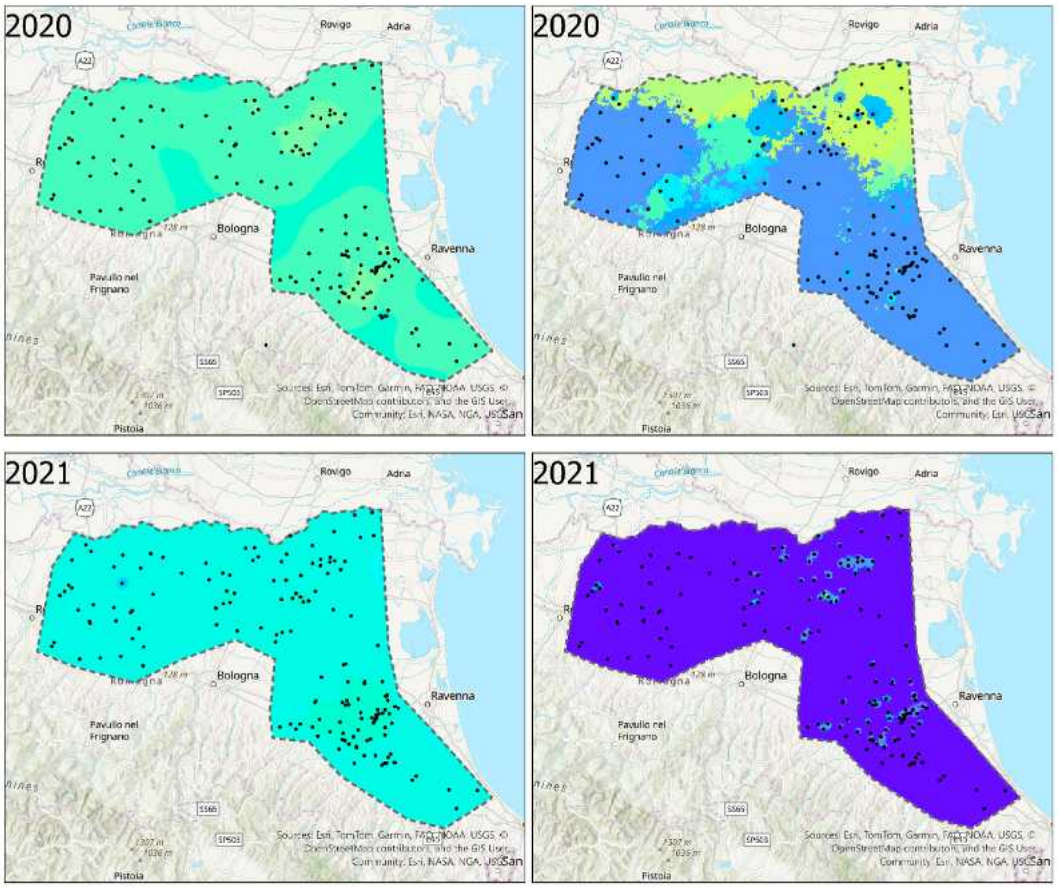

Figure 11. *Cont.*

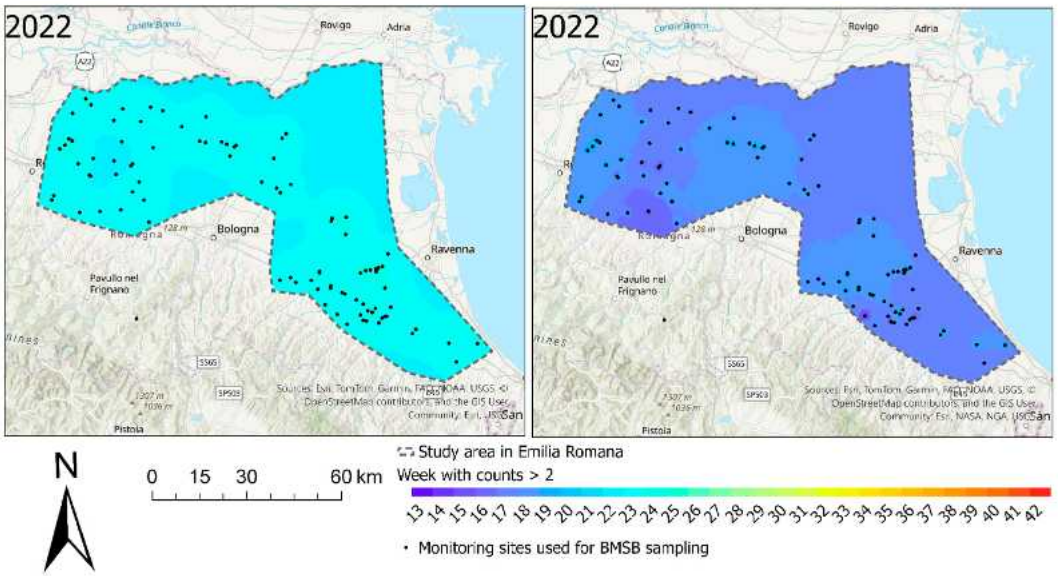

Figure 11. Spatial distribution of week with counts for Small (**left panels**) and Adult (**right panels**) individuals above 2 in 2020, 2021, and 2022.

4. Discussion

The simulations and spatial mean maps (Figures 8 and 9) effectively capture the temporal patterns described in the previous sections, particularly the strong seasonal control on population counts. The Adults tend to appear earlier in the season, typically in lower numbers, then decline and reappear a few months later. Small individuals show a delayed response relative to Adults and are present over a shorter period, generally around four months, whereas Adults may persist for up to 7–8 months. The abrupt disappearance of counts at the end of summer further highlights the strong seasonal constraint on population dynamics. In fact, such seasonal population dynamics are widely reported for BMSB in invaded regions, where population build-up is linked to climatic conditions and host plant availability [11]. This seasonal structure is consistent with the known phenology of BMSB which is strongly regulated by temperature and photoperiod [7]. Notably, life table parameters obtained under outdoor conditions precisely within our study region (Emilia Romagna, northern Italy) demonstrated that BMSB is bivoltine in this area, with the first oviposition occurring in mid-May and an extensive overlap of generations starting in mid-July [36]. These local biological findings perfectly align with our observed 7–8-month Adult persistence, which spans from the spring exit of overwintering individuals to the late summer/autumn activity of the new summer generation. Furthermore, development rates are strongly temperature-dependent, with complete development from egg to Adult occurring in about 33 to 76 days depending on thermal conditions [7], while the rapid decline in population counts at the end of summer matches the reported arrest of nymphal development as the photoperiod falls below critical thresholds in late August As such, this supports the consistent timing of population peaks observed in Figure 6 and Table 2. Also, similar developmental responses dependent on temperature have also been quantified under controlled conditions, confirming the role of temperature accumulation in regulating life cycle progression [37].

In this context, macroclimatic factors such as ambient temperature and photoperiod fundamentally dictate the seasonal timeline of BMSB, regulating crucial biological checkpoints including diapause termination, reproductive activation, and developmental rates [7,11]. Concurrently, Adult dispersal acts as a dynamic spatial link between diverse crop and non-crop habitats, generating broader spatial continuity and driving the continuous recolonization of optimal agricultural zones. On a local scale, parameters such

as immediate host availability, specific orchard composition, and the presence of alternative wild host plants act as ecological sinks that concentrate oviposition and subsequent nymphal development. Consequently, the persistent hotspots identified in this study reflect predictable geographic areas where high-quality host plants, favourable microclimatic shelters, and recurrent Adult aggregations robustly coincide. The spatial pattern of the Small stage is more irregular, consistent with the variogram nugget effect and smaller range. High values frequently occur adjacent to zero counts, suggesting a fragmented distribution in which local peaks may or may not develop further in subsequent weeks. This reflects a high level of spatial and temporal variability, supported by the substantial nugget effect (~40%) observed in Figure 7. This type of spatial aggregation is characteristic of phytophagous insects with localized oviposition behaviour, where the early-stage survival of the insects is dependent on host plant suitability and even the conditions of the microhabitat [12]. In contrast, the "Adult" stage exhibits a more structured and continuous pattern, likely reflecting its longer persistence, which results in smoother spatial and temporal distributions.

This contrast between stages can be explained by ecological differences in mobility and survival rates, with Adults being highly mobile and capable of dispersing across different landscapes, which leads to smoother spatial gradients. On the other hand, early instars are constrained to the vicinity of oviposition sites and also exhibit a more limited mobility, which results in patchy distributions. Similar spatial structuring has been previously reported, where the local environmental conditions and even host plant distribution strongly influenced *H. halys* population patterns [26]. Moreover, the dispersal behaviour of Adults has been documented, with individuals being capable of moving across crop and non-crop habits, which contributes to landscape population connectivity [14,15].

The distinctly broader spatial and temporal continuity exhibited by Adults can be elucidated by a combination of overlapping biological and operational mechanisms. In our study region (Emilia-Romagna, northern Italy), BMSB is strictly bivoltine, with the first ovipositions typically recorded in mid-May and an extensive overlap of generations starting from mid-July [36]. Adult trap captures seamlessly integrate these complex life stages over time, encompassing overwintered individuals emerging in spring, post-diapause Adults dispersing from artificial or natural winter shelters into nearby crops, and new-generation summer Adults produced progressively later in the season. This extensive generational overlap establishes the Adult stage as a highly persistent and ubiquitous component of the field population, capable of spanning up to 7–8 months. Furthermore, their capacity for sustained flight [38] allows Adults to navigate fluidly across complex landscape matrices—including orchards, hedgerows, and alternative host plants—effectively smoothing out localized spatial gradients. In contrast, Small nymphs are heavily constrained by their limited locomotion, remaining localized near the specific oviposition sites chosen by females, and exhibiting shorter stage durations. Their fragmented spatial signature is further exacerbated by a high vulnerability to early-stage environmental mortality and a strict reliance on immediate, high-quality host suitability [36]. This stark contrast between high Adult mobility and restricted juvenile range explains why Adult patterns present as spatially expansive, whereas Small-stage patterns remain highly fragmented.

Crucially, the fragmented distribution observed for Small nymphs requires cautious interpretation, as it likely reflects an interplay between genuine biological constraints and inherent monitoring-related biases. Because early instars lack wings and exhibit reduced mobility, they are sampled with substantially lower efficiency by pheromone-baited traps compared to highly mobile Adults. Furthermore, fine-scale operational variations—such as trap placement within the canopy, localized sampling density, lure degradation rates, and the immediate surrounding vegetational context—can amplify artificial boundaries, generating abrupt differences in capture rates between neighbouring plots. It is therefore

paramount to emphasize that the geostatistical patterns modelled herein reflect trap-capture distributions and relative population intensity rather than absolute, direct ecological population densities.

Both the simulations and the mean maps indicate that the Small stage undergoes two population cycles per year in several areas, although not uniformly across the region. This helps clarify patterns that are less evident in Figure 6, where it is unclear whether the observed dynamics reflect two distinct generations or spatial shifts within a single cycle. Accordingly, the presence of two population increases is consistent with the facultative bivoltine life cycle described for *H. halys* in temperate regions [13]. However, the spatial inconsistency observed in our study suggests that these apparent cycles may result not only from true generational turnover but also from spatial asynchrony among monitoring locations. As such, this distinction is critical, as regional averages may artificially generate bimodal patterns when local populations peak at different times. This analytical distinction carries pivotal implications for IPM strategies; relying exclusively on regional population averages risks misiming management interventions at the farm level, potentially leading to localized control failures. Spatially explicit modelling serves as a robust decision-support tool, enabling surveyors to successfully differentiate zones characterized by synchronized generational development from areas where localized population peaks occur precociously or with a significant delay. This predictive capacity allows for the strategic shift from broad chemical cover sprays toward targeted management actions, such as localized biocontrol releases, mass trapping, or perimeter-focused interventions.

Moreover, Figure 10 shows that maximum Small counts were highest in 2020, forming a broader and more continuous patch in the northwestern part of Emilia-Romagna, together with a distinct hotspot in the south. In subsequent years, this pattern weakened: in 2021 the distribution became more fragmented and point-like, and in 2022, it was even more reduced and localized. Adult patterns broadly followed the same spatial structure. In 2020, high Adult counts were observed across much of the region, largely overlapping with areas of high Small counts. In 2021, this pattern contracted markedly, with higher values mainly restricted to the northwest. By 2022, Adult counts appeared more spatially structured again, with clearer hotspots, particularly in central and northwestern areas. This interannual variability suggests that early-stage population development is more sensitive to environmental conditions than Adult persistence. Additionally, variations in temperature, host availability and early-stage survival rate may influence the strength and spatial extent of population peaks. Additionally, field monitoring has also demonstrated that the population outbreaks of *H. halys* can vary significantly between years due to climatic variability and to landscape context [3]. Nevertheless, the literature has shown that reproductive success and survival of *H. halys* are highly dependent on temperature, with optimal population growth occurring under moderate thermal conditions [19].

A similar temporal signal is evident in the onset of seasonal activity (Figure 11). Adults consistently appear earlier than Small individuals, reflecting their carryover from the previous year. In 2021, Adult emergence occurred earlier and more homogeneously across the study area, whereas in 2022 it followed a similar spatial pattern but with a delay of one to two weeks. In contrast, in 2020—the first year of monitoring—Adult emergence was more spatially heterogeneous, with noticeable delays in the northern part of the region. For Small individuals, onset patterns were generally more homogeneous, with earlier emergence in 2022 compared to 2021 and 2020, when appearance tended to occur later. The observed interannual variations strongly reinforce the role of macroclimatic variability in shaping the phenological responses of BMSB. The precise timing of post-diapause emergence and subsequent reproduction is heavily governed by the interaction between cumulative temperature (degree-days) and photoperiod, both of which exhibit

substantial fluctuations across different geographic locations and years [7,19]. Furthermore, variations in post-diapause dispersal behaviour—frequently triggered by fluctuating spring temperatures—directly influence the spatial heterogeneities observed during early-season population establishment [2]. Additionally, local biological findings in southern Europe demonstrate that as the photoperiod drops below critical thresholds in late August, a definitive arrest in nymphal development occurs [36]. This photoperiodic constraint perfectly explains the abrupt disappearance of juvenile counts observed in our models at the end of the summer.

Although climatic variability represents the most plausible driver for these interannual shifts, it is important to note that our DSS model did not explicitly incorporate climatic variables or environmental covariates as statistical predictors. Instead, temperature and photoperiod data were utilized purely as a biological framework to contextualize and interpret the modelled BMSB phenology. Consequently, their specific effects were not statistically isolated from confounding drivers, such as changing host availability, shifting landscape composition, localized farm management, or sampling variation. Therefore, the influence of climate must be interpreted as a robust mechanistic explanation supported by the established biology of the species, rather than an empirically isolated causal effect.

Overall, the spatial coincidence between the Small and Adults maxima supports the expected continuity between life stages. At the same time, marked interannual variability is evident in both the location and extent of maximum counts, although the northwestern region consistently emerges as a persistent area of higher density.

On the other hand, considering a modelling perspective, these results demonstrate the advantage of integrating spatial and temporal information, with traditional temporal analyses capturing the general phenological pattern but failing to represent local variability. By contrast, geostatistical approaches allow the identification of spatial structure, aggregation patterns, and uncertainty, which are essential for applied insect ecology [29,30]. The use of Direct Sequential Simulation (DSS) further strengthens this approach by preserving local variability while maintaining consistency with observed data. However, unlike deterministic interpolation methods, DSS avoids excessive smoothing and allows the representation of realistic population extremes, which can be particularly relevant for pest management applications.

Several limitations should be considered when interpreting these results. For instance, we can consider first, the pheromone-trap captures that were used as indicators of relative local abundance, recognising that capture rates can be influenced by trap placement, lure performance, surrounding vegetation, and stage-specific detectability. Second, although the monitoring network covered the main fruit-growing areas of Emilia-Romagna, trap density and exact trap locations varied among years, which may affect local comparisons. Third, DSS provides multiple realizations and variance maps that represent spatial uncertainty, but uncertainty was not used here to redesign the monitoring network because the study focused on historical observations. Finally, environmental covariates such as crop distribution, host-plant density, landscape structure, and microclimatic variability were not explicitly included in the model. These factors are therefore discussed as plausible ecological drivers rather than directly tested predictors. To ensure a balanced interpretation of our findings, several inherent limitations must be transparently addressed. First, pheromone-trap data serve as a proxy for relative local abundance rather than absolute population counts, meaning that capture rates remain inherently sensitive to micro-level variables including trap positioning, lure performance, and stage-specific insect detectability. Second, while the monitoring network effectively covered the primary fruit-growing regions of Emilia-Romagna, the total trap density and exact geographic locations fluctuated between years, which may constrain fine-scale historical comparisons across specific coordinates.

Third, while the DSS framework generates multiple stochastic realizations and variance maps that elegantly quantify spatial uncertainty, this uncertainty was not leveraged to structurally optimize or redesign the regional monitoring network, as the primary objective of this study was the retrospective analysis of historical population data. Finally, explicit landscape covariates—such as precise crop layer distributions, wild host-plant density, structural landscape connectivity, and microclimatic variance—were omitted from the geostatistical model. These factors are thus discussed as highly plausible ecological drivers and macro-scale explanations, rather than directly tested, statistically validated predictors.

Also, from an applied perspective, these findings have direct implications for integrated pest management (IPM), considering that the earlier and more persistent presence of Adults highlights the importance of early-season monitoring, while the fragmented distribution of Small stages suggests that interventions targeting early instars or egg stages require high spatial precision. As such, this study has relevance for biological control strategies involving egg parasitoids [20].

Overall, the results indicate that BMSB population dynamics are structured by predictable seasonal processes but strongly modulated by spatial heterogeneity and even interannual variability. In this context, the integration of phenological analysis with spatiotemporal modelling therefore provides a more robust and realistic framework for understanding pest dynamics and improving targeted management strategies.

5. Conclusions

Our study demonstrates that the seasonal dynamics of *H. halys* in Emilia-Romagna are shaped by a combination of consistent phenological succession and a strong spatial heterogeneity. As such, with weekly pheromone-trap data, it was possible to confirm a recurrent developmental sequence, with Small preceding Large by approximately two weeks and Adults appearing after an additional two to three weeks. However, the moderate interstage correlations indicate that regional averages do not fully represent local population dynamics. The 3D spatiotemporal geostatistical model successfully reproduced the main seasonal population waves and highlighted clear differences between developmental stages. For instance, Adults showed broader spatial continuity and longer temporal persistence, whereas Small displayed more fragmented and localized patterns. Overall, by identifying phenological windows, spatial hotspots and areas of uncertainty, this approach can support more precise timing and spatial targeting of biological and chemical interventions within integrated pest management programmes.

Additionally, future developments of this framework should integrate spatially explicit climate forecasts, remote sensing products, and decision-support systems. Incorporating predictive temperature models and real-time photoperiod data will significantly refine the forecasting of critical phenological transitions. Concurrently, the inclusion of high-resolution remote sensing indices and land-use layers will provide a dynamic representation of commercial crop distributions, non-crop vegetation structures, and wild host availability across the landscape. Integrating these diverse data streams into unified operational platforms will enable the generation of real-time risk maps. Ultimately, this approach will support highly adaptive, climate-resilient IPM recommendations, allowing stakeholders to optimize the timing and spatial deployment of targeted management interventions under rapidly changing environmental conditions.

Author Contributions: Conceptualization, L.G., J.A., and M.S.; methodology, L.G. and J.A.; investigation, L.G., L.M., J.A., and M.S.; resources, L.M.; data curation, L.G. and J.A.; writing—original draft preparation, L.G. and A.R.F.C.; writing—review and editing, L.G., J.A., M.S., A.C.M., A.R.F.C., and L.M.; supervision, L.M. All authors have read and agreed to the published version of the manuscript.

Funding: This research received no external funding.

Institutional Review Board Statement: Not applicable.

Informed Consent Statement: Not applicable.

Data Availability Statement: The monitoring data used in this study were provided by CIMICE.NET.

Acknowledgments: We acknowledge Cimice.net for providing the Brown marmorated stink bug trap and capture data. Also, we want to thank the Seequent company for providing academic licenses of Leapfrog Geo to NOVA-FCT. The authors acknowledge the R&D Unit GEOBIOTEC-UID/04035/2025: GeoBioCiências, GeoTecnologias e GeoEngenharias: https://doi.org/10.54499/UID/04035/2025.

Conflicts of Interest: The authors declare no conflicts of interest.

Abbreviation

The following abbreviation is used in this manuscript:

BMSB Brown Marmorated Stink Bug

References

1. Zhu, G.; Bu, W.; Gao, Y.; Liu, G. Potential geographic distribution of *Halyomorpha halys*. *PLoS ONE* **2012**, *7*, e31246. [CrossRef]
2. Inkley, D.B. Characteristics of home invasion by the brown marmorated stink bug. *J. Entomol. Sci.* **2012**, *47*, 125–130. [CrossRef]
3. Maistrello, L.; Vaccari, G.; Caruso, S.; Costi, E.; Bortolini, S.; Macavei, L.; Foca, G.; Ulrici, A.; Bortolotti, P.; Nannini, R.; et al. Monitoring of *Halyomorpha halys* in northern Italy. *J. Pest Sci.* **2017**, *90*, 1231–1244.
4. Donatelli, M.; Magarey, R.D.; Bregaglio, S.; Willocquet, L.; Whish, J.P.M.; Savary, S. Modelling the impacts of pests and diseases on agricultural systems. *Agric. Syst.* **2017**, *155*, 213–224. [CrossRef] [PubMed]
5. Hoebeke, E.R.; Carter, M.E. *Halyomorpha halys*: A polyphagous plant pest from Asia newly detected in North America. *Proc. Entomol. Soc. Wash.* **2003**, *105*, 225–237.
6. Cianferoni, F.; Graziani, F.; Dioli, P.; Ceccolini, F. Review of the occurrence of *Halyomorpha halys* in Italy, with an update of its European and world distribution. *Biologia* **2018**, *73*, 599–607. [CrossRef]
7. Haye, T.; Abdallah, S.; Gariepy, T.; Wyniger, D. Phenology, life table analysis and temperature requirements of *Halyomorpha halys* in Europe. *J. Pest Sci.* **2014**, *87*, 407–418. [CrossRef]
8. Dioli, P.; Leo, P.; Maistrello, L. Prime segnalazioni in Spagna e in Sardegna della specie aliena *Halyomorpha halys* (Stål, 1855) e note sulla sua distribuzione in Europa (Hemiptera, Pentatomidae). *Rev. Gadit. Entomol.* **2016**, *7*, 539–548.
9. Berteloot, O.H.; Kuhn, A.; Peusens, G.; Beliën, T.; Hautier, L.; Van Leeuwen, T.; De Clercq, P. Distribution and genetic diversity of the invasive pest *Halyomorpha halys* (Hemiptera, Pentatomidae) in Belgium. *NeoBiota* **2024**, *90*, 123–138. [CrossRef]
10. Maistrello, L. Case study 2: *Halyomorpha halys* (Stål) in Europe. In *Stink Bugs (Hemiptera: Pentatomidae) Research and Management*; Bueno, A.F., Panizzi, A.R., Eds.; Entomology in Focus; Springer: Cham, Switzerland, 2024; Volume 9, Chapter 15. [CrossRef]
11. Leskey, T.C.; Nielsen, A.L. Impact of the invasive brown marmorated stink bug. *Annu. Rev. Entomol.* **2018**, *63*, 599–618. [CrossRef] [PubMed]
12. Rice, K.B.; Bergh, C.J.; Bergmann, E.J.; Biddinger, D.J.; Dieckhoff, C.; Dively, G.; Fraser, H.; Gariepy, T.; Hamilton, G.; Haye, T.; et al. Biology, ecology, and management of brown marmorated stink bug. *J. Integr. Pest Manag.* **2014**, *5*, A1–A13. [CrossRef]
13. Haye, T.; Gariepy, T.; Hoelmer, K.; Rossi, J.P.; Streito, J.C.; Tassus, X.; Desneux, N. Range expansion of the invasive brown marmorated stink bug. *J. Pest Sci.* **2015**, *88*, 665–673. [CrossRef]
14. Lee, D.H.; Short, B.D.; Joseph, S.V.; Bergh, J.C.; Leskey, T.C. Review of the biology and management of *Halyomorpha halys* in Asia. *Environ. Entomol.* **2013**, *42*, 627–641. [CrossRef] [PubMed]
15. Mohekar, P.; Osborne, J.; Wiman, N.G.; Walton, V.; Tomasino, E. Influence of Winemaking Processing Steps on the Amounts of (E)-2-Decenal and Tridecane as off-Odorants Caused by Brown Marmorated Stink Bug (*Halyomorpha halys*). *J. Agric. Food Chem.* **2017**, *65*, 872–878. [CrossRef] [PubMed]
16. Leskey, T.C.; Hamilton, G.C.; Nielsen, A.L.; Polk, D.F.; Rodriguez-Saona, C.; Bergh, J.C.; Herbert, D.A.; Kuhar, T.P.; Pfeiffer, D.; Dively, G.P.; et al. Pest status of the brown marmorated stink bug, *Halyomorpha halys*, in the USA. *Outlooks Pest Manag.* **2012**, *23*, 218–226. [CrossRef]
17. Henry, M.; Leung, B.; Cuthbert, R.N.; Bodey, T.W.; Ahmed, D.A.; Angulo, E.; Balzani, P.; Briski, E.; Courchamp, F.; Hulme, P.E.; et al. Unveiling the hidden economic toll of biological invasions in the European Union. *Environ. Sci. Eur.* **2023**, *35*, 43. [CrossRef] [PubMed]

18. Bosco, L.; Nardelli, M.; Tavella, L. First Insights on Early Host Plants and Dispersal Behavior of *Halyomorpha halys* (Hemiptera: Pentatomidae) from Overwintering to Crop Colonization. *Insects* **2020**, *11*, 866. [CrossRef] [PubMed]
19. Fouani, J.M.; Scala, M.; Zaffaroni-Caorsi, V.; Verrastro, V.; Anfora, G.; Mazzoni, V. The post-diapause vibrational behavior, motility, and survival of *Halyomorpha halys* adults at different temperatures. *Sci. Rep.* **2024**, *14*, 1198. [CrossRef] [PubMed]
20. Zapponi, L.; Tortorici, F.; Anfora, G.; Bardella, S.; Bariselli, M.; Benvenuto, L.; Bernardinelli, I.; Butturini, A.; Caruso, S.; Colla, R.; et al. Distribution of exotic egg parasitoids of *Halyomorpha halys*. *Insects* **2021**, *12*, 316. [CrossRef] [PubMed]
21. Sorbelli, F.B.; Coro, F.; Das, S.K.; Di Bella, E.; Maistrello, L.; Palazzetti, L.; Pinotti, C.M. A drone-based application for scouting *Halyomorpha halys* bugs in orchards with multifunctional nets. In *Proceedings of the 2022 IEEE International Conference on Pervasive Computing and Communications Workshops (PerCom Workshops 2022)*; IEEE: New York, NY, USA, 2022; pp. 127–129.
22. Forresi, C.; Gallinucci, E.; Golfarelli, M.; Maistrello, L.; Preti, M.; Vaccari, G. A data platform for real-time monitoring and analysis of the brown marmorated stink bug in Northern Italy. *Ecol. Inform.* **2024**, *82*, 102713. [CrossRef]
23. Kuhar, T.P.; Kamminga, K. Review of the chemical control research on *Halyomorpha halys* in the USA. *J. Pest Sci.* **2017**, *90*, 1021–1031. [CrossRef]
24. Talamas, E.J.; Herlihy, M.V.; Dieckhoff, C.; Hoelmer, K.A.; Buffington, M.; Bon, M.C.; Weber, D.C. *Trissolcus japonicus* (Ashmead) (Hymenoptera, Scelionidae) emerges in North America. *J. Hymenopt. Res.* **2015**, *43*, 119–128. [CrossRef]
25. Rondoni, G.; Bertoldi, V.; Malek, R.; Foti, M.C.; Peri, E.; Maistrello, L.; Conti, E. Native egg parasitoids recorded from the invasive *Halyomorpha halys* successfully exploit volatiles emitted by the plant–herbivore complex. *J. Pest Sci.* **2017**, *90*, 1087–1095. [CrossRef]
26. Liakos, V.; Navrozidis, I.E.; Koutsogeorgiou, E.I.; Gogolashvili, N.E.; Samourgkanidou, E.; Faraslis, I.; Gravalos, I.; Thomidis, T.; Andreadis, S.S. Spatiotemporal distribution of *Halyomorpha halys* populations. *Plants* **2023**, *12*, 2282. [CrossRef] [PubMed]
27. ARPAE. 2023. Available online: https://www.arpae.it/it (accessed on 29 April 2026).
28. Heusler, J.; Funk, J.; Wagner, A. Spatial interpolation in applied insect ecology: A review. *J. Appl. Entomol.* **2025**, *149*, 1319–1334. [CrossRef]
29. Sciarretta, A.; Trematerra, P. Geostatistical tools for insect spatial distribution. *Plant Prot. Sci.* **2014**, *50*, 97–110. [CrossRef]
30. Liebhold, A.; Rossi, R.; Kemp, W. Geostatistics and GIS in applied insect ecology. *Annu. Rev. Entomol.* **2003**, *38*, 303–327. [CrossRef]
31. Cressie, N.; Wikle, C.K. *Statistics for Spatio-Temporal Data*; Wiley: New York, NY, USA, 2011.
32. Goovaerts, P. *Geostatistics for Natural Resources Evaluation*; Oxford University Press: New York, NY, USA, 1997.
33. Isaaks, E.H.; Srivastava, R.M. *An Introduction to Applied Geostatistics*; Oxford University Press: New York, NY, USA, 1989.
34. Nunes, R.; Almeida, J. Parallelization of sequential simulation algorithms. *Comput. Geosci.* **2010**, *36*, 1042–1052. [CrossRef]
35. Soares, A. Direct sequential simulation and cosimulation. *Math. Geol.* **2001**, *33*, 911–926. [CrossRef]
36. Costi, E.; Haye, T.; Maistrello, L. Biological parameters of the invasive brown marmorated stink bug, *Halyomorpha halys*, in southern Europe. *J. Pest Sci.* **2017**, *90*, 1059–1067. [CrossRef]
37. Nielsen, A.L.; Hamilton, G.C.; Matadha, D. Developmental rate estimation for *Halyomorpha halys*. *Environ. Entomol.* **2008**, *37*, 348–355. [CrossRef]
38. Wiman, N.G.; Walton, V.M.; Shearer, P.W.; Rondon, S.I.; Lee, J.C. Factors affecting flight capacity of *Halyomorpha halys*. *J. Pest Sci.* **2015**, *88*, 37–47. [CrossRef]